crystals

MDPI

Article

Cocrystals Based on 4,4′-bipyridine: Influence of Crystal Packing on Melting Point

Daniel Ejarque [1], Teresa Calvet [2], Mercè Font-Bardia [3] and Josefina Pons [1,*]

[1] Departament de Química, Universitat Autònoma de Barcelona, Bellaterra, 08193 Barcelona, Spain; daniel.ejarque@uab.cat
[2] Departament de Mineralogia, Petrologia i Geologia Aplicada, Universitat de Barcelona, Martí i Franquès s/n, 08028 Barcelona, Spain; mtcalvet@ub.edu
[3] Unitat de Difracció de Raig-X, Centres Científics i Tecnològics de la Universitat de Barcelona (CCiTUB), Universitat de Barcelona, Solé i Sabarís, 1-3, 08028 Barcelona, Spain; mercef@ccit.ub.edu
* Correspondence: josefina.pons@uab.es; Tel.: +34-935-812-895

Abstract: The reactions of piperonylic acid (HPip) and cinnamic acid (HCinn) with 4,4′-bipyridine (4,4′-bipy) have been assayed using the same synthetic methodology, yielding two binary cocrystals with different acid:4,4′-bipy molar ratios, (HPip)(4,4′-bipy) (**1**) and $(HCinn)_2$(4,4′-bipy) (**2**). The melting point (m.p.) of these cocrystals have been measured and a remarkable difference ($\Delta T \approx 78$ °C) between them was observed. Moreover, the two cocrystals have been characterized by powder X-ray diffraction (PXRD), elemental analysis (EA), FTIR-ATR, ^{1}H NMR spectroscopies, and single-crystal X-ray diffraction. The study of their structural packings *via* Hirshfeld surface analysis and energy frameworks revealed the important contribution of the $\pi\cdots\pi$ and C-H$\cdots\pi$ interactions to the formation of different structural packing motifs, this being the main reason for the difference of m.p. between them. Moreover, it has been observed that **1** and **2** presented the same packing motifs as the crystal structure of their corresponding carboxylic acids, but **1** and **2** showed lower m.p. than those of the carboxylic acids, which could be related to the lower strength of the acid-pyridine heterosynthons respect to the acid-acid homosynthons in the crystal structures.

Keywords: cocrystals; 4,4′-bipyridine; piperonylic acid; cinnamic acid; acid-pyridine heterosynthon; X-ray crystal structures; melting point; Hirshfeld surface analysis; energy frameworks

Citation: Ejarque, D.; Calvet, T.; Font-Bardia, M.; Pons, J. Cocrystals Based on 4,4′-bipyridine: Influence of Crystal Packing on Melting Point. *Crystals* **2021**, *11*, 191. https://doi.org/10.3390/cryst11020191

Academic Editor: Abel Moreno
Received: 28 January 2021
Accepted: 13 February 2021
Published: 16 February 2021

1. Introduction

Over the last 50 years, crystal engineering has emerged as an interdisciplinary field between crystallography and chemistry through the rationalization of crystal structures from the molecular and supramolecular assemblies [1,2]. For this purpose, the study of strong and recurrent patterns of supramolecular interactions, known as supramolecular synthons, has allowed the control and prediction of the assembly of Active Pharmaceutical Ingredients (APIs) with guest molecules (coformers) [3]. Within this frame, multicomponent solids comprising salts and cocrystals have inspired great interest owing to their ability to enhance the physicochemical properties of APIs [4]. In addition, the classification of intermolecular interactions into supramolecular synthons has allowed for simplifying the extended scaffold of multicomponent solids into modular units, facilitating their study [5] and the better understanding of the relationship between structural packing and their effects on different physicochemical (melting point [6], solubility [7] or stability [8], among others [9–14]) and mechanical properties [15,16].

In this sense, the appropriate selection of the starting molecules for the controlled formation of either cocrystals or salts is usually done bearing in mind the pKa values of the starting materials. In fact, there is a rule of thumb that dictates, depending on the ΔpKa value (ΔpKa = pKa[protonated base] - pKa[acid]), the proton will remain in the acid (ΔpKa < 0) resulting in a cocrystal, or it will be placed in the base (ΔpKa > 3.75) obtaining

a salt [17–19]. In addition, there are intermediate cases where ΔpKa is between 0 and 3.75 and the pKa rule cannot be applied successfully, since the location of the proton is sometimes challenging because it is between the acid and the base forming a salt-cocrystal continuum [20,21].

Among all cocrystals, those containing carboxylic acids are widely studied because they are commonly found in APIs [22–24]. Therefore, the study of cocrystals formed by carboxylic acids is useful when relating to the effects of supramolecular interactions in properties. Furthermore, carboxylic acids and pyridine derivatives are usually combined for the obtention of cocrystals due to the possibility of predicting their main interaction through the formation of the robust and recurrent acid-pyridine heterosynthon [25,26].

Previously, our group obtained a binary cocrystal based on the acid-amide heterosynthon composed of two 1,3-benzodioxole-5-carboxylic acid molecules (piperonylic acid, HPip) and one isonicotinamide molecule (Isn) with formula $(HPip)_2(Isn)$ [27]. As a continuation, in this contribution, we have selected the 4,4′.bipyridine (4,4′-bipy) as a coformer and the HPip and *trans*-3-phenylacrylic acid (cinnamic acid, HCinn) molecules to synthesize two cocrystals based on the acid-pyridine heterosynthon. Following the same synthetic methodology, two binary cocrystals with different acid:4,4′-bipy molar ratios have been obtained, (HPip)(4,4′-bipy) (**1**) and $(HCinn)_2$(4,4′-bipy) (**2**) (Scheme 1). The melting point values of both have been measured and their difference with respect to the starting materials has been studied in terms of crystal packing through the analysis of their corresponding crystalline structures. Moreover, Hirshfeld surface analysis, energy frameworks, and lattice energy calculations have been used for better understanding the measured melting point values.

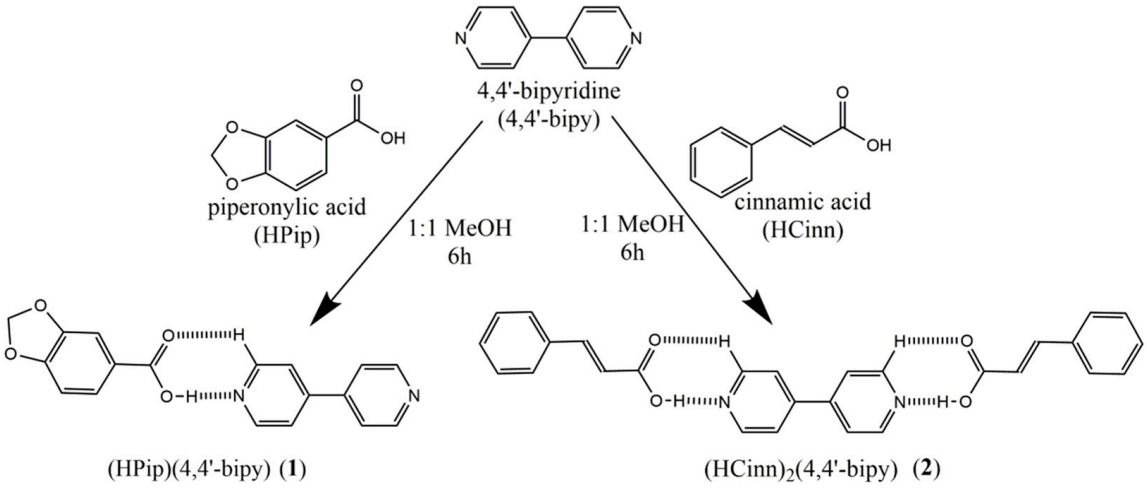

Scheme 1. Outline of the synthetic methodologies for obtaining cocrystals (HPip)(4,4′-bipy) (**1**) and $(HCinn)_2$(4,4′-bipy) (**2**).

2. Experimental Section

2.1. Materials and General Methods

1,3-benzodioxole-5-carboxylic acid (piperonylic acid, HPip), *trans*-3-phenylacrylic acid (cinnamic acid, HCinn), 4,4′-bipyridine (4,4′-bipy), and methanol (MeOH) as solvent were purchased from Sigma-Aldrich. Deuterated dimethylsulfoxide (dmso-d_6) was used for the NMR experiments and was purchased from Eurisotop (Saint-Aubin, France). All of them were used without further purification. All the reactions and manipulations were carried out in air at room temperature (RT). Powder X-ray diffraction (PXRD) patterns were measured with a PANalytical X'Pert PRO MPD θ/θ powder diffractometer of a 240 millimeter radius, in a configuration convergent beam with a focalizing mirror and a transmission geometry with flat samples sandwiched between low absorbing films. A CuKα radiation with λ = 1.5418 Å was used (45 kW and 40 mA). All of them were recorded from 2θ = 2° to 60° with a step scan of 0.0263° and a measuring time of 300 s per step.

Melting points (m.p.) were measured on a Stuart Melting Point Apparatus SMP30 (Cole-Parmer, UK), using a 2.0 °C/min step rate from RT to 200 °C. Elemental analyses (C, H, N) were carried on a Euro Vector 3100 instrument. FTIR-ATR spectra were recorded on a Tensor 27 (Bruker) spectrometer, equipped with an attenuated total reflectance (ATR) accessory model MKII Golden Gate with a diamond window in the range 4000–500 cm^{-1}. ^1H NMR spectra were recorded on an NMR-FT Bruker 360 and 400 MHz spectrometers in dmso-d_6 solutions at RT. All chemical shifts (δ) are given in ppm relative to TMS as the internal standard.

*2.2. Synthesis of Cocrystals **1** and **2***

For cocrystal **1**, equimolar quantities of HPip (101 mg, 0.608 mmol) and 4,4′-bipy (95.0 mg, 0.608 mmol) were dissolved in 15 mL of MeOH at RT and stirred for six hours. The resulting colorless solution was concentrated under vacuum until a white crystalline solid precipitated. The obtained solid was filtered and dried under vacuum. The synthesis of **2** was performed by the same methodology but using HCinn instead of HPip.

Suitable colorless crystals of **1** and **2** were obtained by slow evaporation of the mother liquors in air for seven (**1**) or eight (**2**) days.

1. Isolated Yield: 111 mg (56.8%). M.p. 188-189 °C. Elemental analysis calc(%) for $C_{18}H_{14}N_2O_4$ (322.31): C 67.08; H 4.38; N 8.69; found: C 66.94; H 4.27; N 8.54. FTIR-ATR (wavenumber, cm^{-1}): 3085-3026(w) [ν(C-H)$_{ar}$], 2986-2919(w) [ν(C-H)$_{al}$], 2782(w), 2597-2165(br) [ν(O-H)], 1980-1771(br) [ν(OH···N)], 1699(w) [ν(COOH)], 1690(w), 1626(w), 1592(w) [ν(C=C/C=N)], 1538(w), 1498(m) [δ(C=C/C=N)], 1435(w), 1408(w), 1360(w), 1287(m), 1261(s), 1243(m), 1214(m), 1162(m) [ν(C-O-C)], 1108(m), 1072(m), 1034(m) [δ(C-H)$_{ip}$], 1014(m) [δ(C-H)$_{ip}$], 989(w), 933(m), 914(m), 880(w), 852(w), 832(w), 808(s) [δ(C-H)$_{oop}$], 776(w), 761(s) [δ(C-H)$_{oop}$], 734(w), 718(w), 668(w), 621(s), 567(w), 528(m). ^1H NMR (360 MHz; dmso-d_6; Me_4Si; 298 K): δ = 12.79 [1H, s, COO*H*$_{HPip}$], 8.73 [4H, d, ^3J = 4.2 Hz, *o*-*H*$_{4,4'\text{-bipy}}$], 7.83 [4H, d, ^3J = 4.5 Hz, *m*-*H*$_{4,4'\text{-bipy}}$], 7.54 [1H, d, ^3J = 8.1 Hz, HOOC−C−C*H*−CH$_{HPip}$], 7.36 [1H, s, HOOC−C−C*H*−CO$_{HPip}$], 7.00 [1H, d, ^3J = 8.1 Hz, HOOC−C−CH−C*H*$_{HPip}$], 6.12 [2H, s, O−C*H*$_2$−O$_{HPip}$].

2. Isolated Yield: 95.5 mg (61.9%). M.p. 110-111 °C. Elemental analysis calc(%) for $C_{28}H_{24}N_2O_4$ (452.50): C 74.32; H 5.35; N 6.19; found: C 74.05; H 5.18; N 6.02. FTIR-ATR (wavenumber, cm^{-1}): 3068-3026(w) [ν(C-H)$_{ar}$], 2985-2896(w) [ν(C-H)$_{alk}$], 2795(w), 2673(w), 2583-2166(br) [ν(O-H)], 2029-1787(br) [ν(OH···N)], 1688(m) [ν(COOH)], 1633(m), 1594(m) [ν(C=C/C=N)], 1532(w), 1490(w), 1447(w), 1406(s) [δ(C=C/C=N)], 1327(m), 1308(m), 1280(m), 1205(m), 1190(s), 1160(w), 1074(w), 1061(m) [δ(C-H)$_{ip}$], 1040(w), 988(s) [δ(C-H)$_{ip}$], 965(m), 872(w), 851(w), 802(s) [δ(C-H)$_{oop}$], 765(s) [δ(C-H)$_{oop}$], 719(m), 708(w), 690(s), 685(s), 630(w), 619(w), 608(m), 572(w), 524(m). ^1H NMR (400 MHz; dmso-d_6; Me_4Si; 298 K): δ = 12.37 [2H, s, COO*H*$_{HCinn}$], 8.72 [4H, d, ^3J = 5.7 Hz, *o*-*H*$_{4,4'\text{-bipy}}$], 7.82 [4H, d, ^3J = 5.7 Hz, *m*-*H*$_{4,4'\text{-bipy}}$], 7.67 [4H, d, ^3J = 6.2 Hz, *o*-*H*$_{HCinn}$], 7.59 [2H, d, ^3J = 16.0 Hz, HOOC−CH−C*H*$_{HCinn}$], 7.41 [6H, m, *m*-*H*$_{HCinn}$ + *p*-*H*$_{HCinn}$], 6.53 [2H, d, ^3J = 16.0, HOOC−C*H*−CH$_{HCinn}$].

2.3. X-ray Crystallographic Data

For cocrystals **1** and **2**, colorless prism-like specimens were used for the X-ray crystallographic analysis. The X-ray intensity data was measured on a D8 Venture system equipped with a multilayer monochromate and a Mo microfocus (λ = 0.71073 Å). For all the compounds, the frames were integrated with the Bruker SAINT Software Package using a narrow-frame algorithm. For **1**, the H atoms were located on a difference synthesis and refined with an isotropic temperature factor equal to 1.2, the equivalent temperature factor of the atom was linked, and 13 H atoms were computed and refined, using a riding model, with an isotropic temperature factor equal to 1.2, the equivalent temperature factor of the atom which was linked and thus, the bond lengths of X-H were fixed. Moreover, the H atom bound to O have been refined without AFIX, and the difference electron density appeared at 0.9 Å from O atom and at 1.5 Å from N atom. For **2**, all the other hydrogen atoms were

refined using a riding model (AFIX) with an isotropic temperature factor equal to 1.2, the equivalent temperature factor of the atom to which are linked, and thus, the bond lengths of X-H were fixed. For **1**, the integration of the data using a monoclinic unit cell yielded a total of 20300 reflections to a maximum θ angle of 26.40° (0.80 Å resolution), of which 2999 were independent (average redundancy 6.769, completeness = 99.8%, R_{int} = 6.40%, R_{sig} = 4.15%) and 2456 (81.89%) were greater than 2σ(|F|^2). The calculated minimum and maximum transmission coefficients (based on crystal size) are 0.6133 and 0.7474. For **2**, the integration of the data using a monoclinic unit cell yielded a total of 18015 reflections to a maximum θ angle of 30.91° (0.69 Å resolution), of which 3609 were independent (average redundancy 4.992, completeness = 98.1%, R_{int} = 7.78%, R_{sig} = 6.91%) and 2136 (59.19%) were greater than 2σ(|F|^2). The calculated minimum and maximum transmission coefficients (based on crystal size) are 0.6585 and 0.7461 (Table 1). The temperature used for performing these experiments was 100(2) K.

Table 1. Crystal data and structure refinement for **1** and **2**.

	1	**2**
CCDC	2058460	2058461
Empirical Formula	$C_{18}H_{14}N_2O_4$	$C_{28}H_{24}N_2O_4$
Formula weight	322.31	452.49
T (K)	100(2)	100(2)
Wavelength (Å)	0.71073	0.71073
System, space group	Monoclinic, $P2_1/c$	Monoclinic, $P2_1/n$
a (Å)	3.7524(6)	7.8058(10)
b (Å)	18.427(3)	7.1639(8)
c (Å)	21.139(3)	20.786(3)
α (°)	90	90
β (°)	92.646(6)	93.147(5)
γ (°)	90	90
V (Å^3)	1460.1(4)	1160.6(3)
Z	4	2
D_{calc} (mg/m^3)	1.466	1.295
μ (mm^{-1})	0.105	0.087
F (000)	672	476
Crystal size (mm^3)	0.208 × 0.039 × 0.036	0.270 × 0.120 × 0.090
hkl ranges	−4<=h<=4, −23<=k<=23, −26<=l<=26	−11<=h<=11, −10<=k<=10, −29<=l<=29
θ range (°)	2.210 to 26.402	2.741 to 30.909
Reflections collected/unique/[R_{int}]	20300 / 2999 / [R_{int}] = 0.0640	18015 / 3609 / [R_{int}] = 0.0778
Completeness to θ (%)	99.8	99.9
Absorption correction	Semi-empirical from equivalents	Semi-empirical from equivalents
Max. and min. transmission	0.7474 and 0.6133	0.7461 and 0.6585
Refinement method	Full-matrix least-squares on $\|F\|^2$	Full-matrix least-squares on $\|F\|^2$
Data/Restrains/Parameters	2999 / 0 / 221	3609 / 0 / 157
Goodness-on-fit (GOF) on $\|F\|^2$	1.107	1.063
Final R indices [I>2σ(I)]	R_1 = 0.0539	R_1 = 0.0553
	wR_2 = 0.1113	wR_2 = 0.1108
R indices (all data)	R_1 = 0.0692	R_1 = 0.1229
	wR_2 = 0.1174	wR_2 = 0.1507
Extinction coefficient	n/a	0.019(3)
Largest diff-peak and hole (e. Å^{-3})	0.232 and −0.290	0.301 and −0.297

The structures were solved and refined using the Bruker SHELXTL Software package and refined using SHELX (version 2018/3) [28]. For **1**, the final anisotropic full-matrix least-squares refinement on |F|^2 with 221 variables converged at R_1 = 5.39% for the observed data and wR_2 = 11.74% for all data. For **2**, the final anisotropic full-matrix least-squares refinement on |F|^2 with 157 variables converged at R_1 = 5.53% for the observed data and wR_2 = 15.07% for all data. For **1** and **2**, the final cell constants and volume are based upon the refinement of the XYZ-centroids of reflections above 2θ σ(I). Data were corrected

for absorption effects using the Multi-Scan method (SADABS). Crystal data and relevant details of structure refinement for compounds **1** and **2** are reported in Table 1. Molecular graphics were generated using Mercury (version 4.3.1) [29–31] with POV-Ray Package (version 3.7) [32]. Color codes for all molecular graphics: red (O), light blue (N), dark grey (C), and white (H).

2.4. Computational Details of Hirshfeld Surface Analysis, Energy Frameworks, and Lattice Energy

Hirshfeld surface analysis and energy frameworks of the two cocrystals have been performed with CrystalExplorer 17.5 [33]. Hirshfeld surfaces, combined with 2D fingerprint plots, are a powerful graphical tool to evaluate the supramolecular interactions present in crystal structures. The surface mapping facilitates their identification while the fingerprint plot outlines the distances between the atoms involved in these contacts. Owing to the multicomponent nature of cocrystals, the Hirshfeld surfaces of the components have been calculated independently for each different molecule of the unit cell using an isovalue of 0.5 e·au^{-3}.

Moreover, all the crystal structures have been analyzed by energy frameworks analysis with TONTO [34], using the CE-B3LYP/6-31G(d,p) energy model, starting from the .cif files obtained from the single-crystal X-ray diffraction data. The energy framework is a unique tool to visualize the supramolecular architecture of crystal structures. The total energy (E_{tot}) is divided into electrostatic (E_{ele}), polarization (E_{pol}), dispersion (E_{dis}), and repulsion (E_{rep}) contribution energies, in which cylinders represent the relative strength of the molecular packing and have been fixed at a scale factor of 150 to make their comparison possible. All the different molecules confined in a cluster of 20 Å in the unit cell, including those crystallographically independent, have been used for the interaction energy calculations. The contribution of all the molecular pairs themselves and with the neighboring ones, as well as the contributions of the nearby molecules themselves, were included, ensuring that at a higher radius the total energies did not differ more than 1 KJ/mol [35].

The obtention of the total energy for each particular interaction can be achieved by applying Equation (1), where scale factors are applied for each contribution in order to calibrate the energy values against B3LYP-D2/6-31G(d,p) interaction energies, as implemented in CrystalExplorer 17.5 [35,36].

$$E_{tot} = E_{ele}+E_{pol}+E_{dis}+E_{rep} = 1.057E'_{ele}+0.740E'_{pol}+0.871E'_{dis}+0.618E'_{rep} \quad (1)$$

Furthermore, the calculation of the total interaction energies between each molecular pair allows the obtention of the lattice energy (E_{lat}) of each structure applying Equation (2), where N_i is the number of molecule pairs in the cluster with that interaction energy and E_i is the interaction energy value [37].

$$E_{lat} = \frac{1}{2}\sum_{i=1}^{n}(N_i \cdot E_i) \quad (2)$$

3. Results and Discussion

*3.1. Synthesis and Characterization of Cocrystals **1** and **2***

Cocrystals **1** and **2** have been afforded by mixing the corresponding carboxylic acids (HPip, **1**; HCinn, **2**) with 4,4′-bipyridine in a 1:1 molar ratio using MeOH as solvent at RT. The resulting products consist of two binary cocrystals, one with 1:1 (**1**) and the other with 2:1 (**2**) acid:4,4′-bipy molar ratios. The pKa values of the starting molecules (4,4′-bipy: 3.17, 4.82; HPip: 4.35; HCinn: 4.46), allow us to calculate the corresponding ΔpKa parameters ($pKa_{1(4,4'\text{-bipy})} - pKa_{carboxylic\ acid}$), both lying in the ΔpKa < 0 range (**1**: −1.18; **2**: −1.29). Therefore, the obtention of cocrystals is expected [17].

Cocrystals **1** and **2** were characterized by powder X-ray diffraction (PXRD), melting point (m.p.), elemental analysis (EA), FTIR-ATR, and ^{1}H NMR spectroscopies. Detailed information is provided in the Supporting Information (Figures S1–S5). Furthermore, single crystals suitable for the X-ray diffraction method have been obtained. The m.p.

values are 188–189 °C (**1**) and 110−111 °C (**2**), showing a difference of ΔT ≈ 78 °C between them and exhibiting displacement with respect to the corresponding starting materials. G.L. Perlovich compiled a complete database quantifying over a large number of cocrystal structures the number of cocrystals with m.p. lying between the starting molecules (55.3%), below (28.9%) and beyond (15.8%) them [38]. Based on this database, the m.p. of **1** lies in the more usual case, since it is placed between the values of the former molecules. Conversely, cocrystal **2** presents a m.p. lower than HCinn and 4,4′-bipy, probably due to their weaker intermolecular interactions compared with the crystalline structure of the starting molecules [39,40].

The crystal structure of both cocrystals has been elucidated by single-crystal X-ray diffraction and then, analyzed and discussed using the graph set descriptors developed by M.C. Etter. In both structures, the patterns have only been reduced into supramolecular rings (R) and the notation has been given as $R_d^a(n)$, where "a" represents the number of H-bond acceptors, "d" is the number of H-bond donors and "n" is the minimum number of atoms for completing the supramolecular rings [41,42].

*3.2. Crystal and Extended Structure of (HPip)(4,4′-bipy) (**1**)*

Cocrystal **1** belongs to the monoclinic $P2_1/c$ space group. It consists of a binary cocrystal containing one HPip and one 4,4′-bipy molecule associated through an HPip-4,4′-bipy heterosynthon with $R_2^2(7)$ graph set descriptor (O1-H1···N1, 1.62(4) Å, 172(3)°; C13-H13···O2, 2.95 Å, 121°) (Table 2; Figure 1a). It is noteworthy to mention that to the best of our knowledge [43], a few numbers of cocrystal structures containing 4,4′-bipy and carboxylic acids present the recurrent acid-pyridine heterosynthon only through one of their nitrogen atoms, while the other displays a weak C-H···N interaction [44,45]. Moreover, the bond lengths of C-O (1.323(3) Å) and C=O (1.221(3) Å) of the carboxylic acid confirm that the cocrystal has been obtained. These bond lengths conjointly with the interaction parameters of the heterosynthon are similar to other reported binary 1:1 cocrystals [44,45].

Table 2. Selected supramolecular interactions for cocrystal **1**.

D-H···A	D-H (Å)	H···A (Å)	D···A (Å)	> D-H···A (°)
O(1)-H(1)···N(1)	0.99(3)	1.62(4)	2.603(2)	172(3)
C(13)-H(13)···O(2)	0.95	2.95	3.540(3)	121
C(4)-H(4)···O(3)	0.95	2.69	3.612(2)	164
C(6)-H(6AB)···N(2)	0.99	2.58	3.348(3)	134
C(12)-H(12)···O(2)	0.95	2.47	3.369(3)	159
C(15)-H(15)···O(2)	0.95	2.45	3.395(3)	173
C(10)-H(10)···O(4)	0.95	2.47	3.326(3)	150
C(6)-H(6A)···N(2)	0.99	2.73	3.589(3)	146

Cg(I)···Cg(J)	d_{Cg-Cg} [a] (Å)	α [b] (°)	β, γ [c] (°)	$d_{plane-plane}$ [d]	d_{offset} [e]
Cg(1)···Cg(1)	3.7523(13)	0	28.4	3.3021(8)	1.782
Cg(2)···Cg(2)	3.7524(14)	0	20.3	3.5187(9)	1.304
Cg(3)···Cg(3)	3.7523(13)	0	20.6	3.5113(9)	1.323

[a] Centroid-centroid distance. [b] Dihedral angle between the ring planes. [c] Offset angles: angle between Cg(I)-Cg(J) vector and normal to plane I, angle between Cg(I)-Cg(J) vector and normal to plane J (β = γ, when α = 0). [d] Perpendicular distance of Cg(I) on plane J and perpendicular distance of Cg(J) on plane I (equal when α = 0). [e] Horizontal displacement or slippage between Cg(I) and Cg(J) (equal for both centroids when α = 0). Cg(1) = C(2) C(3) C(4) C(5) C(7) C(8); Cg(2) = N(1) C(9) C(10) C(11) C(12) C(13); Cg(3) = N(2) C(14) C(15) C(16) C(17) C(18).

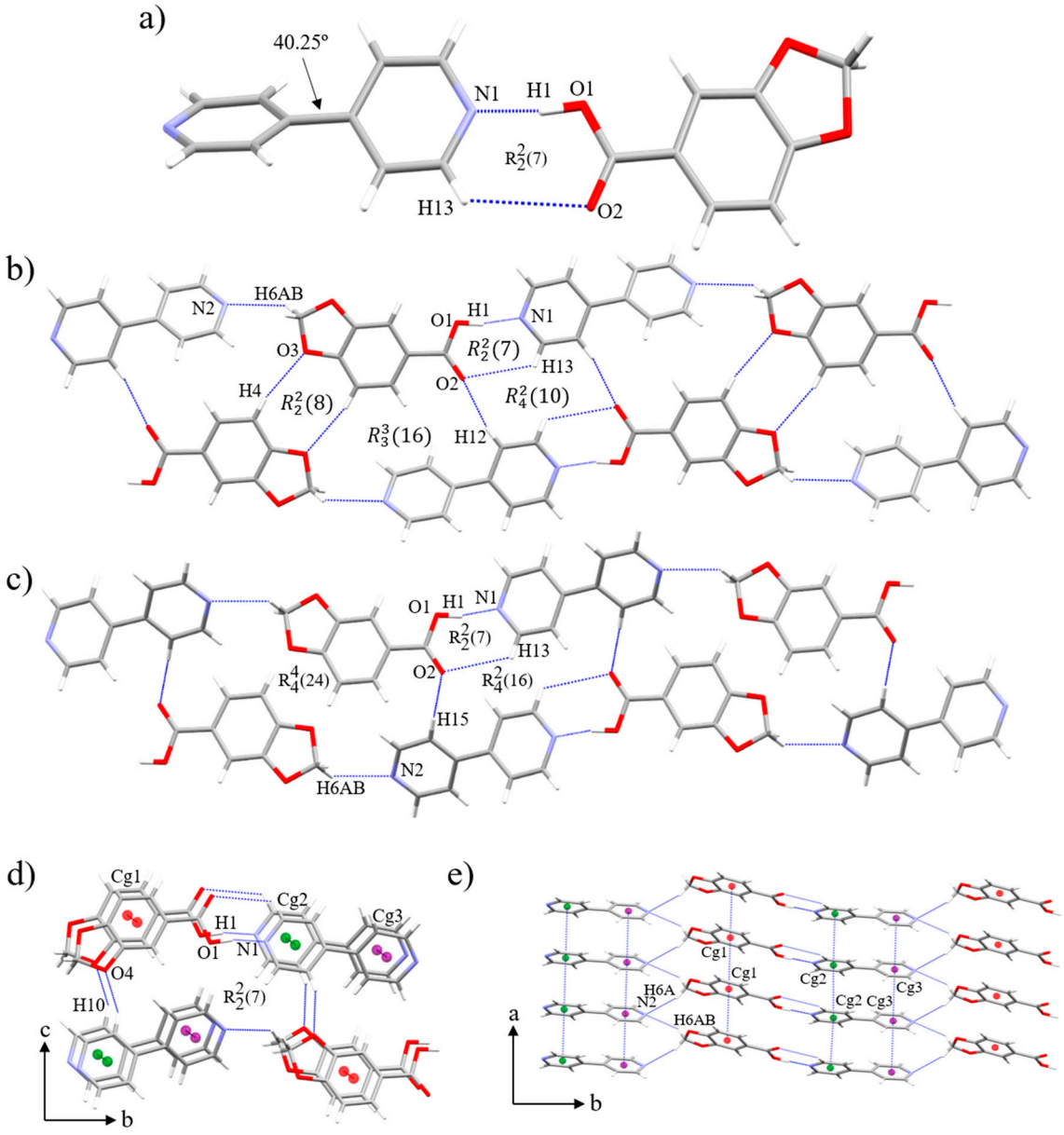

Figure 1. (**a**) Structure of cocrystal (HPip)(4,4′-bpy) (**1**). (**b**) Chain 1 and (**c**) chain 2 of cocrystal **1**, both expanding along the $[\bar{1}10]$ and [110] directions. (**d**) General view along the *bc* plane of the C10-H10···O4 which expands the structure through the *c* axis. (**e**) General view of the C-H···N and π···π interactions of cocrystal **1** along the *ab* plane.

Cocrystal **1** expands its structure through the formation of two different chains (1 and 2) promoted by the torsion of the 4,4′-bipy rings (40.25°), whose interactions extend the crystal structure along the $[\bar{1}10]$ and [110] directions. Chain 1 is composed of three supramolecular rings with graph set descriptors, $R_2^2(8)$, $R_3^3(16)$, and $R_4^2(10)$. The $R_2^2(8)$ motif is formed by two interactions between the *m*-H of the HPip and a dioxole oxygen atom (C4-H4···O3, 2.69 Å, 164°). The $R_3^3(16)$ motif contains one of the previous C4-H4···O3 interactions together with a C-H···N association between a dioxole proton and one of the nitrogen atoms from a 4,4′-bipy (C6-H6AB···N2, 2.58 Å, 134°), and a C-H···O interaction between a *m*-H from a 4,4′-bipy and the carboxylic oxygen atom not involved in the HPip-4,4′-bipy heterosynthon (C12-H12···O2, 2.47 Å, 159°). Furthermore, the third supramolecular ring, presenting a $R_4^2(10)$ motif contains two C12-H12···O2 and two C13-H13···O2 interactions from the heterosynthons (Figure 1b).

Chain 2 is formed by two different supramolecular rings with graph set descriptors $R_4^2(16)$ and $R_4^4(24)$. The $R_4^2(16)$ motif combines de C-H···O interaction from the heterosynthon with another C-H···O association promoted by a *m*-H atom from the 4,4′-bipy and a dioxole oxygen atom (C15-H15···O2, 2.45 Å, 173°), whereas the $R_4^4(24)$ motif is formed by the previously mentioned C15-H15···O2 and C6-H6AB···N2 interactions (Figure 1c). Furthermore, both chains are connected along the *c* axis through a C10-H10···O4 interaction between a third *m*-H atom from the 4,4′-bipy with the other dioxole oxygen atom (C10-H10···O4, 2.47 Å, 150°) (Figure 1d).

Finally, the structure is expanded along the *a* axis through three π···π interactions (Cg1···Cg1, 3.7523(13) Å, Cg2···Cg2, 3.7524(14) Å, Cg3···Cg3, 3.7523(13) Å) (Table 2; Figure 1e) [46]. These interactions are supported by two C-H···N interactions promoted by the two dioxole hydrogen atoms with the nitrogen atoms not involved in the HPip-4,4′-bipy heterosynthon (C6-H6AB···N2; C6-H6A···N2, 2.73 Å, 146°). In addition, the *m*-H atoms of the 4,4′-bipy involved in the formation of chain 1 and 2 (C12-H12···O2 and C15-H15···O2) held two HPip molecules together, one above the other, facilitating the π ··π stackings. All this set of interactions promotes the formation of a 3D network with a lamellar motif.

*3.3. Crystal and Extended Structure of (HCinn)$_2$(4,4′-bipy) (**2**)*

Cocrystal **2** belongs to the monoclinic $P2_1/n$ space group. It consists of a binary cocrystal containing two HCinn and one completely plane 4,4′-bipy molecules associated through two HCinn-4,4′-bipy heterosynthons (O1-H1···N003, 1.61(2) Å, 178.4(14)°; C10-H10···O2, 2.57 Å, 126°), both forming the characteristic $R_2^2(7)$ graph set descriptor (Table 3; Figure 2a). The bond lengths of C-O (1.325(2) Å) and C=O (1.224(2) Å) of the carboxylic acid group conjointly with the interaction parameters of the HCinn-4,4′-bipy heterosynthon are similar to other reported binary 2:1 cocrystals and confirm that the cocrystal has been obtained [47,48].

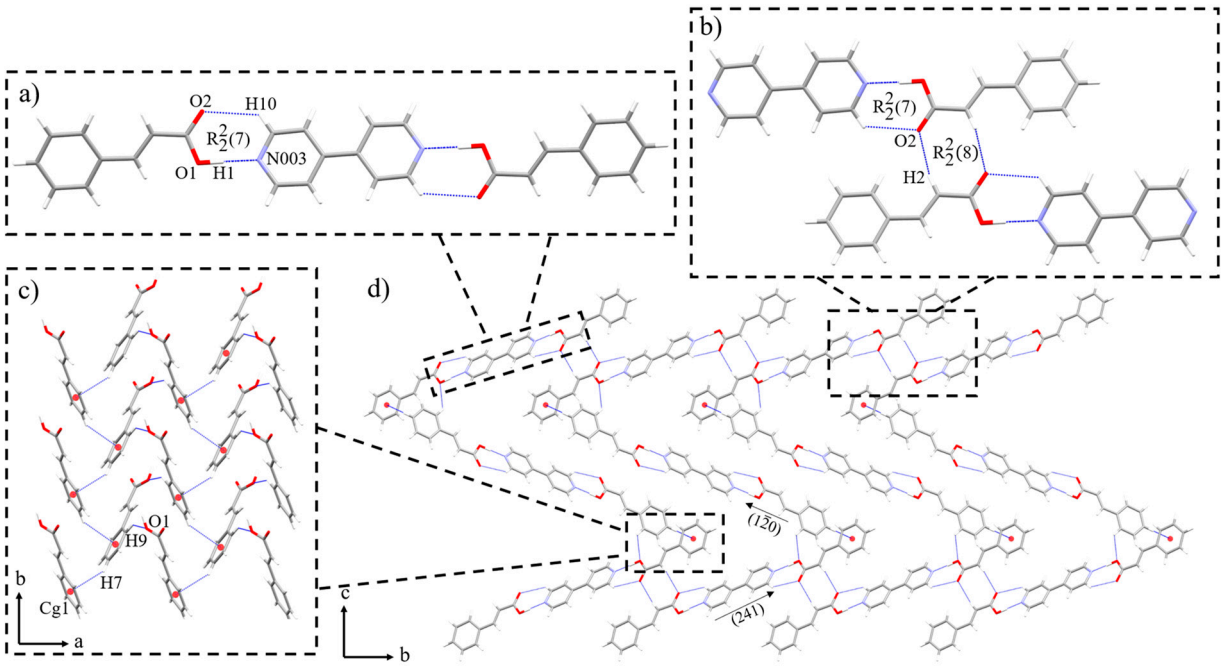

Figure 2. (**a**) Structure of cocrystal (HCinn)$_2$(4,4′-bpy) (**2**). (**b**) Supramolecular interactions which expand the structure of **2** through the [1$\bar{2}$0] and [241] directions. (**c**) View along the *ab* plane of the C-H···π and C-H···O interactions between HCinn molecules connecting the chains which expand the structure through the [1$\bar{2}$0] and [241] directions. (**d**) General view of the supramolecular structure of **2** along the *bc* plane.

Table 3. Selected supramolecular interactions for cocrystal **2**.

D-H···A	D-H (Å)	H···A (Å)	D···A (Å)	> D-H···A (°)
O(1)-H(f··N(003)	1.03(2)	1.61(2)	2.636(2)	178.4(14)
C(10)-H(10)···O2	0.95	2.57	3.227(2)	126
C(2)-H(2)···O(2)	0.95	2.47	3.381(2)	160
C(9)-H(9)···O(1)	0.95	2.68	3.401(2)	133
C(7)-H(7)···Cg(1)	0.95	2.95	3.770(2)	146

Cg(1) = C(4) C(5) C(6) C(7) C(8) C(9).

Cocrystal **2** forms chains in the $[1\bar{2}0]$ and [241] directions through the HCinn-4,4′-bipy heterosynthon combined with a double hydrogen bond with $R_2^2(8)$ graph set descriptor formed between the oxygen atom from the carboxylic groups which does not participate in the HCinn-4,4′-bipy heterosynthon and one of the hydrogen atoms from the double bonds of HCinn placed nearer to the carboxylic moieties (C2-H2···O2, 2.47 Å, 160°) (Figure 2b). Furthermore, the two chains with different crystallographic directions are connected between them by a C-H···π and a C-H···O interactions. The C-H···π interaction joints the *p*-H atoms of HCinn with the aromatic rings of nearby HCinn molecules (C7-H7···Cg1, 2.95 Å, 146°), while the C-H···O interaction supports the connection of the chains by the association of two HCinn molecules through an *o*-H atom and a protonated oxygen atom from the carboxylic group (C9-H9···O1, 2.68 Å, 133°) (Figure 2c). These sets of interactions expand the structure of **2** forming *zig-zag* chains along the *bc* plane, which are held together through the *a* axis by the C9-H9···O1 and C7-H7···Cg1 interactions, forming a herringbone motif 3D network (Figure 2d).

*3.4. Hirshfeld Surface Analysis and Energy Frameworks Calculations of **1** and **2***

The Hirshfeld surfaces and 2D fingerprint plots of **1** and **2** were analyzed for the identification of the main intermolecular interactions, which will provide us a better overview of the contribution of the different atoms of each molecule in the crystal packing. Detailed information of the d_{norm} and curvedness mappings of the different molecules of both cocrystals as well as a chart representation of the percentages of Hirshfeld surface of each molecule of **1** and **2** is provided in the Supporting Information (Figures S6–S8).

The 2D fingerprint plots of both cocrystals show the COOH···N heterosynthon as the more important interaction with a prominent spike with $d_e+d_i \approx 1.6$ Å (Figure 3a,b). The fingerprint plot of **1** contains in its H···N/N···H contacts the heterosynthon interaction and the two C-H···N associations involving the dioxole hydrogen atoms, while in the same type of contacts of **2**, only the heterosynthon is observed. Therefore, the direct comparison between the heterosynthons is difficult to achieve based only on the percentage of Hirshfeld surface and we can only observe that H···N/N···H contacts in **1** are more important than in **2**.

When the H···O contacts of both cocrystal were analyzed, a spike with a higher d_e+d_i length of **1** with respect to **2** was found (**1**: 2.5 Å; **2**: 2.3 Å). The comparison of the percentage of H···O contacts in HPip and HCinn carboxylic acids show similar values (**1**: 5.7%; **2**: 5.9%), probably because there is a competence between the nearer interaction of **1** and the higher number of interactions in **2**. By contrast, the H···O contacts of 4,4′-bipy fingerprint plots clearly show how the number of interactions in **1** rises the percentage value when compared with **2** (**1**: 14.8%; **2**: 9.7%) (Figure 3c,d). Furthermore, the O···H interactions show similar lengths around $d_e+d_i \approx 2.3$ Å, where the same trend as in the H···O contacts is also observed (**1**: 26.7%; **2**: 12.8%) (Figure 3e,f).

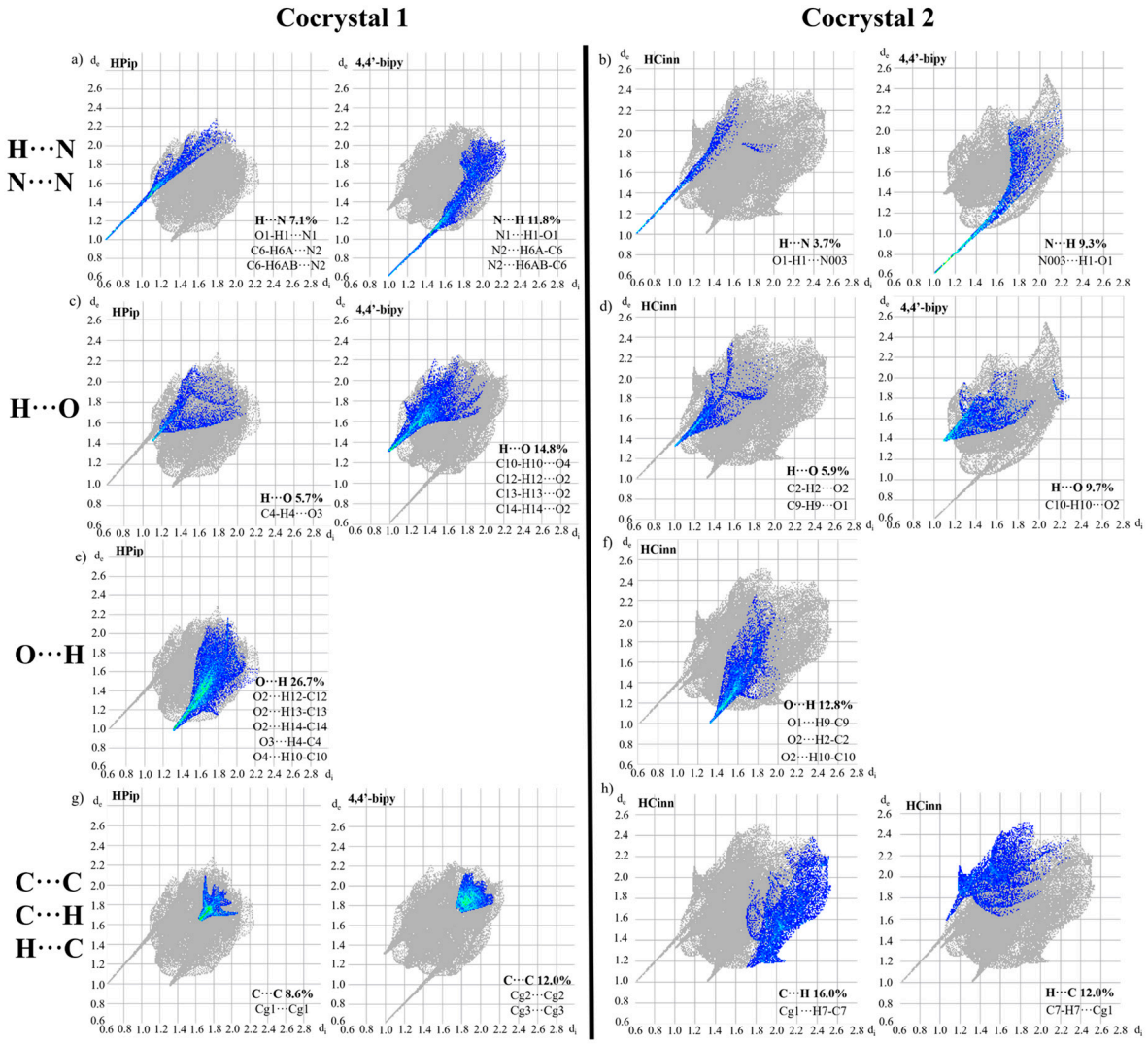

Figure 3. 2D fingerprint plots of H···N/N···H contacts in (**a**) **1** and (**b**) **2**. H···O contacts in (**c**) **1** and (**d**) **2**. O···H contacts in (**e**) **1** and (**f**) **2**. (**g**). C···C contacts in **1** and (**h**) C···H/H···C contacts in **2**.

The last interactions to analyze for both cocrystals were those involving aromatic rings. For **1**, a well-defined region is observed when the C···C of the HPip and 4,4′-bipy molecules are represented (Figure 3g). The higher number of π···π interactions in 4,4′-bipy over HPip is also in accordance with the higher percentage of C···C contacts in 4,4′-bipy (12.0%) with respect to HPip (8.6%). Moreover, the analysis of the 2D fingerprint plots of cocrystal **2** revealed the characteristic "wings" shape in the HCinn molecules either through the C···H (16.0%) as well as for the H···C (12.0%) contacts, suggesting the presence of C-H···π interactions (Figure 3h) [49].

Aiming to better understand the structural packing of both cocrystals by comparing the different contribution energies, energy framework contributions have been calculated. The energy frameworks of **1** and **2** exhibited that the electrostatic contribution is the most important energy component, since the molecular pairs joined by the heterosynthons outstands are represented as the biggest red cylinders. Therefore, their contribution in the associated total energies of −46.1 (**1**) and −48.9 (**2**) KJ/mol should be a majority. Moreover, **2** presents other remarkable red cylinders that joint the molecular pairs forming a *zig-zag* energy topology (SI: Table S1) [50]. Despite **1** not presenting other remarkable cylinders, the number of weaker interactions related with small cylinders with associated total energies between −16.2 and −8.8 KJ/mol is considerably higher and form various *zig-zag* energy

topologies, which could be promoted by the torsion of the 4,4′-bipy and the presence of the dioxole hydrogen atoms in HPip (Figure 4a,b).

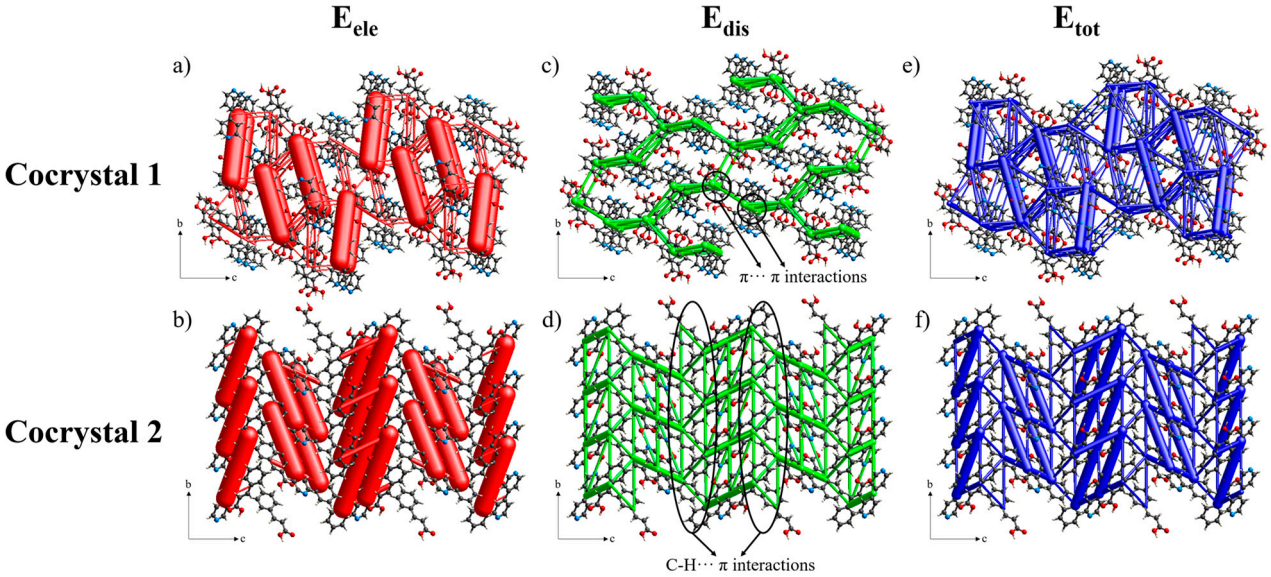

Figure 4. Energy frameworks (E_{ele}, E_{dis}, and E_{tot}) for cocrystals **1** and **2**. All the diagrams use the same energy cylinder scale factor of 150 and an energy cut-off of 6.00 KJ/mol within a 2 × 1 × 2 (**1**) and a 3 × 3 × 3 (**2**) unit cells. Electrostatic energy of (**a**) **1** and (**b**) **2**. Dispersion energy of (**c**) **1** and (**d**) **2**. Total energy of (**e**) **1** and (**f**) **2**.

The dispersion forces, though less significant, are essential in the crystal packing of both cocrystals, since they assemble the chains formed by electrostatic contribution energies. For **1**, the dispersion interactions are attributed to the three π···π interactions which should be the main contributors to the associated total energies of −25.8 KJ/mol and −23.4 KJ/mol (Figure 4c), while for **2** these forces are ascribed to C-H···π interactions with a major contribution in an associated total energy value significantly lower of −10.8 KJ/mol (Figure 4d).

The total energy representation showed an overall view of the different energetic contributions. In these representations, it is observed how **1** sustain its 3D framework by a more crowded array formed by the HPip-4,4′-bipy heterosynthons, a high number of weak interactions forming various *zig-zag* energy topologies, and three π···π interactions being part of cylinders with an intermediate strength between those where the heterosynthon and the C-H···O interactions mainly contribute (Figure 4e). On the other hand, cocrystal **2** presented a less crowded energy framework where the HCinn-4,4′-bipy heterosynthons, a lower number of weak interactions forming also *zig-zag* energy topologies, and C-H···π interactions being part of cylinders with significantly lower associated total energy compared with the previous π···π interactions, held the 3D network together (Figure 4f).

Finally, the obtention of the total energy for each particular interaction allows us to calculate the lattice energy (E_{lat}) of **1** and **2** to ensure they are thermodynamically more favorable than the crystal structures of the starting materials [51,52]. The calculated values were −225.4 KJ/mol (**1**) and −333.7 KJ/mol (**2**) being like other 1:1 and 2:1 cocrystals [53–55]. Considering the ratio of the molecules of **1** and **2**, the obtained lattice energies are lower than the sum of the lattice energies of the starting materials (Table 4). Detailed information of the overall contribution energies used for the lattice energy calculations are provided in the Supporting Information (Table S2).

Table 4. Lattice energy (E_{lat}) of the crystal structures of the starting materials and cocrystals **1** and **2**. All the values have been obtained using CrystalExplorer 17.5 from the corresponding .cif files.

Structure	CCDC Number	E_{lat} (KJ/mol)
4,4'-bipy	131130 [56]	−93.8
HPip	608427 [57]	−121.2
HCinn	1547787 [58]	−115.6
1	2058460	−225.4
2	2058461	−333.7

*3.5. Relationship of Melting Point Values with Packing Effects of Cocrystals **1** and **2***

The comparison between **1** and **2** and with their starting materials was performed to try to find some explanations for their m.p. values based on crystal packing effects. For this purpose, the crystal densities and the packing efficiencies have been obtained from the crystallographic data of **1** and **2**, and from the crystal structures of the starting materials (Table 5) [43].

Table 5. Structural parameters and melting point values of 4,4'-bipy, HPip and HCinn crystal structures, and cocrystals **1** and **2**.

Structure	CCDC Number	Melting Point (°C)	Crystal Density (mg/m^3)	Packing Efficiency (%)
4,4'-bipy	131130 [56]	112–113	1.255	68.00
HPip	608427 [57]	231–232	1.555	72.63
HCinn	1547787 [58]	135–136	1.321	70.96
1	2058460	188–189	1.466	73.79
2	2058461	110–111	1.295	69.63

The crystal structure of HPip and HCinn carboxylic acids present acid-acid homosynthons having a major contribution in cylinders with considerably higher associated total energy (HPip: −84.5; HCinn: −79.7 KJ/mol) compared with the corresponding acid-pyridine heterosynthons (**1**: −46.1; **2**: −48.9 KJ/mol) (SI: Table S3; Figures S9–S10). These acid-acid homosynthons conjointly with other weak C-H···O interactions form 1D chains in HPip and HCinn crystal structures contributing to the energy associated to cylinders with similar total energy values. Therefore, the comparison of these chains with respect to those of **1** and **2**, shows how the presence of the acid-acid homosynthons should have an important effect on the m.p. values, since it has a major contribution in an associated total energy value ≈1.6–1.8 times higher than the corresponding heterosynthons. Moreover, if we study the interactions that connect their supramolecular chains, we observe that HPip shows strong π···π interactions (mostly contributing to the cylinder with the total energy of −35.6 KJ/mol) forming a lamellar motif, while HCinn presents weaker C-H···π interactions (−9.5 KJ/mol) showing a herringbone motif. The different packings between the two carboxylic acids could also affect the m.p. of HPip over HCinn, which is also in accordance with their crystal density and packing efficiency values (Table 5).

When the 3D networks of the two cocrystals have been analyzed, the same structural motifs as in the corresponding starting carboxylic acids have been observed. Herein, the different structural motifs promoted by the different planar interactions are suggested as the main contributors responsible for the difference in m.p. between **1** and **2**, as it happens with the comparison between the carboxylic acids [59,60]. These differences are also reflected in the crystal density and packing efficiency values, being higher in **1** with respect to **2**. In fact, when the cylinders with the same direction as the planar interactions of the cocrystals are compared with those of their corresponding carboxylic acids, we found that the difference of associated total energy values in **1** (−25.8 and −23.4 KJ/mol) with respect to HPip (−35.6 KJ/mol) is more important than between **2** (−10.8 KJ/mol) and HCinn (−9.5 KJ/mol). These differences could explain the different m.p. values

between the cocrystals and their precursor carboxylic acids, being higher in **1** respect to **2** ($\Delta T \approx 43$ °C (**1**) and 25 °C (**2**)).

Finally, the crystal structure of 4,4′-bipy has been analyzed and compared with **2** (SI: Table S3; Figure S11). The structure of 4,4′-bipy is held together by different C-H···N interactions forming a 2D plane, while the 3D network is obtained through different π···π interactions. Otherwise, we have seen that **2** expands its structure through the HCinn-4,4′-bipy heterosynthon and different C-H···O interactions forming chains, that combined with C-H···π interactions expands to a 3D network. The presence of the acid-pyridine heterosynthon in **2** may favor the higher m.p. of **2** over 4,4′-bipy. Nonetheless, the presence of π···π interactions expanding the structure of 4,4′-bipy forming a 3D network against the C-H···π interactions which form the 3D network in **2** could be again an important factor which equilibrates the m.p. values. Bearing in mind the completely different structural packings of both crystal structures, a specific reason to explain the m.p. similarities was difficult to be found although the mentioned contributions should have an influence on the obtained values.

4. Conclusions

Two cocrystals have been obtained using 4,4′-bipy as a coformer and HPip and HCinn carboxylic acids, presenting an important m.p. difference ($\Delta T \approx 78$ °C). The reactions have been carried out through the same methodology, but cocrystals with different acid:4,4′-bipy molar ratios were obtained, (HPip)(4,4′-bipy) (**1**) and $(HCinn)_2$(4,4′-bipy) (**2**). It is noteworthy that cocrystal **1** shows an unusual behavior of the 4,4′-bipy since it does not form the classical double acid-pyridine heterosynthon.

The calculated lattice energies indicate that the formation of the two cocrystals is thermodynamically favored over the crystal structure of the starting molecules. Moreover, the FTIR-ATR spectra allow the identification of the acidic proton located in the carboxylic acids by the assignation of the ν(O-H), ν(OH···N) and ν(COOH) signals, while the ^{1}H NMR revealed the 1:1 and 2:1 molar ratios of **1** and **2**, respectively.

The study of the crystal structures supported by Hirshfeld surface analysis show how cocrystal **1** expands its framework through COOH···N, C-H···O and π···π interactions forming a lamellar motif, while for **2** the propagation of the structure is promoted by COOH···N, C-H···O and C-H···π interactions resulting in a herringbone motif. Furthermore, energy frameworks outstand the energetic difference between the π···π interactions of **1** and the C-H···π interactions of **2**, which are responsible for connecting the different chains in both cocrystals. The different motifs promoted by these planar interactions as well as the strength ascribed to them are the factors that explain the high difference in m.p. of **1** respect **2**, while the lower acid-pyridine heterosynthons strengths in respect to the acid-acid homosynthons could explain the lower m.p. values of the cocrystals in respect to the starting carboxylic acids. Therefore, a clear example where the influence of planar interactions in the structural packing of cocrystals is reflected on the properties of these compounds, promoting an important difference in the m.p. values. Differences in the crystal packing arrays such as those explained in this contribution could be extrapolated to other pharmaceutical cocrystals whose crystal structures have not been elucidated yet.

Supplementary Materials: The following are available online at https://www.mdpi.com/2073-4352/11/2/191/s1, Figure S1. PXRD patterns of cocrystal **1** and **2** and XRD data collected from the crystal structures of **1** and **2** and their starting molecules. Figures S2 and S3: FTIR-ATR spectra of **1** and **2**; Figures S4 and S5: ^{1}H NMR spectra of **1** and **2**. Figure S6 and S7: Hirshfeld surfaces of **1** and **2**; Figure S8: Percentage contribution to the Hirshfeld surface for the different molecules of **1** and **2**. Figure S9-S11: Crystal structures of HPip, HCinn and 4,4′-bipy with their corresponding energy frameworks diagrams; Table S1: Associated total energy values of the individual intermolecular interactions of **1** and **2**; Table S2: Contribution, total and lattice energies of the crystal structures of the starting materials and cocrystals **1** and **2**; Table S3: Associated total energy values of the individual intermolecular interactions of the crystal structures of HPip, HCinn and 4,4′-bipy. Complete infor-

mation about the crystal structure and molecular geometry is available in .cif format as Supporting Information.

Author Contributions: Conceptualization, J.P.; methodology, D.E.; software, D.E.; validation, J.P. and T.C.; formal analysis, D.E. and M.F.-B; investigation, D.E.; resources, J.P. and T.C.; data curation, D.E. and M.F.-B.; writing—original draft preparation, D.E.; writing—review and editing, J.P.; visualization, D.E.; supervision, J.P.; project administration, J.P.; funding acquisition, J.P. All authors have read and agreed to the published version of the manuscript.

Funding: This work was financed by the CB615921 project, the CB616406 project from "Fundació La Caixa" and the 2017SGR1687 project from the Generalitat de Catalunya. D.E. acknowledges the PIF pre-doctoral fellowship from the Universitat Autònoma de Barcelona.

Conflicts of Interest: The authors declare no conflict of interest.

References

1. Braga, D.; Grepioni, F. Reactions between or within molecular crystals. *Angew. Chem. Int. Ed.* **2004**, *43*, 4002–4011. [CrossRef] [PubMed]
2. Desiraju, G.R. Crystal engineering: From molecule to crystal. *J. Am. Chem. Soc.* **2013**, *135*, 9952–9967. [CrossRef]
3. Desiraju, G.R. Supramolecular Synthons in Crystal Engineering-A New Organic Synthesis. *Angew. Chem. Int. Ed.* **1995**, *34*, 2311–2327. [CrossRef]
4. Karimi-Jafari, M.; Padrela, L.; Walker, G.M.; Croker, D.M. Creating cocrystals: A review of pharmaceutical cocrystal preparation routes and applications. *Cryst. Growth Des.* **2018**, *18*, 6370–6387. [CrossRef]
5. Desiraju, G.R. The Supramolecular Synthon in Crystal Engineering. In *Stimulating Concepts in Chemistry*; Vögtle, F., Stoddart, J.F., Shibasaki, M., Eds.; Wiley-VCH: Weinheim, Germany, 2000; pp. 293–306.
6. Nayak, A.; Pedireddi, V.R. Rational Analysis of Melting Point Behavior of Co-Crystals of 4-Nitrophenol with Some Aza-Compounds. *Cryst. Growth Des.* **2016**, *16*, 5966–5975. [CrossRef]
7. Thakuria, R.; Delori, A.; Jones, W.; Lipert, M.P.; Roy, L.; Rodríguez-Hornedo, N. Pharmaceutical cocrystals and poorly soluble drugs. *Int. J. Pharm.* **2013**, *453*, 101–125. [CrossRef]
8. Vangala, V.R.; Chow, P.S.; Tan, R.B.H. Characterization, physicochemical and photo-stability of a co-crystal involving an antibiotic drug, nitrofurantoin, and 4-hydroxybenzoic acid. *CrystEngComm* **2011**, *13*, 759–762. [CrossRef]
9. Schultheiss, N.; Newman, A. Pharmaceutical cocrystals and their physicochemical properties. *Cryst. Growth Des.* **2009**, *9*, 2950–2967. [CrossRef] [PubMed]
10. Bolla, G.; Nangia, A. Pharmaceutical cocrystals: Walking the talk. *Chem. Commun.* **2016**, *52*, 8342–8360. [CrossRef] [PubMed]
11. Kale, D.P.; Zode, S.S.; Bansal, A.K. Challenges in Translational Development of Pharmaceutical Cocrystals. *J. Pharm. Sci.* **2017**, *106*, 457–470. [CrossRef] [PubMed]
12. Sun, L.; Wang, Y.; Yang, F.; Zhang, X.; Hu, W. Cocrystal Engineering: A Collaborative Strategy toward Functional Materials. *Adv. Mater.* **2019**, *31*, 1–22. [CrossRef] [PubMed]
13. Thakuria, R.; Sarma, B. Drug-Drug and Drug-Nutraceutical Cocrystal/Salt as Alternative Medicine for Combination Therapy: A Crystal Engineering Approach. *Crystals* **2018**, *8*, 101. [CrossRef]
14. Feiler, T.; Bhattacharya, B.A.L.; Michalchuk, A.; Schröder, V.; List-Kratochvil, E.; Emmerling, F. Mechanochemical Syntheses of Isostructural Luminescent Cocrystals of 9-Anthracenecarboxylic Acid with two Dipyridines Coformers. *Crystals* **2020**, *10*, 889. [CrossRef]
15. Arkhipov, S.G.; Losev, E.A.; Nguyen, T.T.; Rychkov, D.A.; Boldyreva, E.V. A large anisotropic plasticity of L-leucinium hydrogen maleate preserved at cryogenic temperatures. *Acta Cryst.* **2019**, *B75*, 143–151. [CrossRef]
16. Ahmed, E.; Karothu, D.P.; Naumov, P. Crystal Adaptronics: Mechanically Reconfigurable Elastic and Superelastic Molecular Crystals. *Angew. Chem. Int. Ed.* **2018**, *57*, 8837–8846. [CrossRef]
17. Bhogala, B.R.; Basavoju, S.; Nangia, A. Tape and layer structures in cocrystals of some di- and tricarboxylic acids with 4,4′-bipyridines and isonicotinamide. From binary to ternary cocrystals. *CrystEngComm* **2005**, *7*, 551–562. [CrossRef]
18. Cruz-Cabeza, A.J. Acid–base crystalline complexes and the pKa rule. *CrystEngComm* **2012**, *14*, 6362–6365. [CrossRef]
19. Kumar, S.; Nanda, A. Approaches to Design of Pharmaceutical Cocrystals: A Review. *Mol. Cryst. Liq. Cryst.* **2018**, *667*, 54–77. [CrossRef]
20. Rajput, L.; Banik, M.; Yarava, J.R.; Joseph, S.; Pandey, M.K.; Nishiyama, Y.; Desiraju, G.R. Exploring the salt-cocrystal continuum with solid-state NMR using natural-abundance samples: Implications for crystal engineering. *IUCrJ* **2017**, *4*, 466–475. [CrossRef] [PubMed]
21. Tothadi, S.; Shaikh, T.R.; Gupta, S.; Dandela, R.; Vinod, C.P.; Nangia, A.K. Can We Identify the Salt–Cocrystal Continuum State Using XPS? *Cryst. Growth Des.* **2021**, *21*, 735–747. [CrossRef]
22. Basavoju, S.; Boström, D.; Velaga, S.P. Pharmaceutical cocrystal and salts of norfloxacin. *Cryst. Growth Des.* **2006**, *6*, 2699–2708. [CrossRef]

23. Ferretti, V.; Dalpiaz, A.; Bertolasi, V.; Ferraro, L.; Beggiato, S.; Spizzo, F.; Spisni, E.; Pavan, B. Indomethacin co-crystals and their parent mixtures: Does the intestinal barrier recognize them differently? *Mol. Pharm.* **2015**, *12*, 1501–1511. [CrossRef]
24. Banik, M.; Gopi, S.P.; Ganguly, S.; Desiraju, G.R. Cocrystal and salt forms of furosemide: Solubility and diffusion variations. *Cryst. Growth Des.* **2016**, *16*, 5418–5428. [CrossRef]
25. Steiner, T. Competition of hydrogen-bond acceptors for the strong carboxyl donor. *Acta Cryst.* **2001**, *B57*, 103–106. [CrossRef]
26. Chen, P.; Zhang, Z.; Parkin, S.; Zhou, P.; Cheng, K.; Li, C.; Yu, F.; Long, S. Preferred formation of the carboxylic acid-pyridine heterosynthon in 2-anilinonicotinic acids. *RSC Adv.* **2016**, *6*, 81101–81109. [CrossRef]
27. Sánchez-Férez, F.; Ejarque, D.; Calvet, T.; Font-Bardia, M.; Pons, J. Isonicotinamide-Based Compounds: From Cocrystal to Polymer. *Molecules* **2019**, *24*, 4169. [CrossRef]
28. Sheldrick, G.M. A short history of SHELX. *Acta Cryst.* **2008**, *A64*, 112–122. [CrossRef] [PubMed]
29. Macrae, C.F.; Edgington, P.R.; McCabe, P.; Pidcock, E.; Shields, G.P.; Taylor, R.; Towler, M.; van de Streek, J. Mercury: Visualization and analysis of crystal structures. *J. Appl. Cryst.* **2006**, *39*, 453–457. [CrossRef]
30. Macrae, C.F.; Bruno, I.J.; Chisholm, J.A.; Edgington, P.R.; McCabe, P.; Pidcock, E.; Rodriguez-Monge, L.; Taylor, R.; van de Streek, J.; Wood, P.A. Mercury CSD 2.0 – new features for the visualization and investigation of crystal structures. *J. Appl. Cryst.* **2008**, *41*, 466–470. [CrossRef]
31. MacRae, C.F.; Sovago, I.; Cottrell, S.J.; Galek, P.T.A.; McCabe, P.; Pidcock, E.; Platings, M.; Shields, G.P.; Stevens, J.S.; Towler, M.; et al. Mercury 4.0: From visualization to analysis, design and prediction. *J. Appl. Cryst.* **2020**, *53*, 226–235. [CrossRef]
32. Persistence of Vision Pty. Ltd. *Persistence of Vision (TM) Raytracer*; Persistence of Vision Pty. Ltd.: Williamstown, Australia, 2004; Available online: http://www.povray.org/ (accessed on 28 January 2021).
33. Turner, M.J.; McKinnon, J.J.; Wolff, S.K.; Grimwood, D.J.; Spackman, P.R.; Jayatilaka, D.; Spackman, M.A. CrystalExplorer17 (2017). University of Western Australia. Available online: https://crystalexplorer.scb.uwa.edu.au/ (accessed on 28 January 2021).
34. Jayatilaka, D.; Grimwood, D.J. Tonto: A Fortran Based Object-Oriented System for Quantum Chemistry and Crystallography. *Comput. Sci. ICCS* **2003**, *4*, 142–151.
35. Mackenzie, C.F.; Spackman, P.R.; Jayatilaka, D.; Spackman, M.A. CrystalExplorer model energies and energy frameworks: Extension to metal coordination compounds, organic salts, solvates and open-shell systems. *IUCrJ* **2017**, *4*, 575–587. [CrossRef]
36. Thomas, S.P.; Spackman, P.R.; Jayatilaka, D.; Spackman, M.A. Accurate Lattice Energies for Molecular Crystals from Experimental Crystal Structures. *J. Chem. Theory Comput.* **2018**, *14*, 1614–1623. [CrossRef]
37. Spackman, M.A. Towards the use of experimental electron densities to estimate reliable lattice energies. *CrystEngComm* **2018**, *20*, 5340–5347. [CrossRef]
38. Perlovich, G.L. Thermodynamic characteristics of cocrystal formation and melting points for rational design of pharmaceutical two-component systems. *CrystEngComm* **2015**, *17*, 7019–7028. [CrossRef]
39. Nanubolu, J.B.; Ravikumar, K. Correlating the melting point alteration with the supramolecular structure in aripiprazole drug cocrystals. *CrystEngComm* **2016**, *18*, 1024–1038. [CrossRef]
40. Roy, P.; Ghosh, A. Mechanochemical cocrystallization to improve the physicochemical properties of chlorzoxazone. *CrystEngComm* **2020**, *22*, 4611–4620. [CrossRef]
41. Etter, M.C. Encoding and Decoding Hydrogen-Bond Patterns of Organic Compounds. *Acc. Chem. Res.* **1990**, *23*, 120–126. [CrossRef]
42. Bernstein, J.; Davis, R.E.; Shimoni, L.; Chang, N. Patterns in Hydrogen Bonding: Functionality and Graph Set Analysis in Crystals. *Angew. Chem. Int. Ed. Engl.* **1995**, *34*, 1555–1573. [CrossRef]
43. Groom, C.R.; Bruno, I.J.; Lightfoot, M.P.; Ward, S.C. The Cambridge structural database. *Acta Cryst.* **2016**, *B72*, 171–179. [CrossRef]
44. Wicker, J.G.P.; Crowley, L.M.; Robshaw, O.; Little, E.J.; Stokes, S.P.; Cooper, R.I.; Lawrence, S.E. Will they co-crystallize? *CrystEngComm* **2017**, *19*, 5336–5340. [CrossRef]
45. Mukherjee, A.; Desiraju, G.R. Synthon polymorphism and pseudopolymorphism in co-crystals. The 4,4′-bipyridine–4-hydroxybenzoic acid structural landscape. *Chem. Commun.* **2011**, *47*, 4090–4092. [CrossRef]
46. Khavasi, H.R.; Mir Mohammad Sadegh, B. Effect of robust π–π stacking synthon on the formation of mercury coordination compounds; an unusual pseudo-square planar geometry. *Dalton Trans.* **2014**, *43*, 5564–5573. [CrossRef] [PubMed]
47. Tothadi, S. Polymorphism in cocrystals of urea:4,4′-bipyridine and salicylic acid:4,4′-bipyridine. *CrystEngComm* **2014**, *16*, 7587–7597. [CrossRef]
48. Surov, A.O.; Simagina, A.A.; Manin, N.G.; Kuzmina, L.G.; Churakov, A.V.; Perlovich, G.L. Fenamate cocrystals with 4,4′-bipyridine: Structural and thermodynamic aspects. *Cryst. Growth Des.* **2015**, *15*, 228–238. [CrossRef]
49. Spackman, M.A.; McKinnon, J.J. Fingerprinting intermolecular interactions in molecular crystals. *CrystEngComm* **2002**, *4*, 378–392. [CrossRef]
50. Dey, D.; Bhandary, S.; Thomas, S.P.; Spackman, M.A.; Chopra, D. Energy frameworks and a topological analysis of the supramolecular features in in situ cryocrystallized liquids: Tuning the weak interaction landscape via fluorination. *Phys. Chem. Chem. Phys.* **2016**, *18*, 31811–31820. [CrossRef]
51. Chan, H.C.S.; Kendrick, J.; Neumann, M.A.; Leusen, F.J.J. Towards ab initio screening of co-crystal formation through lattice energy calculations and crystal structure prediction of nicotinamide, isonicotinamide, picolinamide and paracetamol multi-component crystals. *CrystEngComm* **2013**, *15*, 3799–3807. [CrossRef]

52. Taylor, C.R.; Day, G.M. Evaluating the Energetic Driving Force for Cocrystal Formation. *Cryst. Growth Des.* **2018**, *18*, 892–904. [CrossRef] [PubMed]
53. Issa, N.; Karamertzanis, P.G.; Welch, G.W.A.; Price, S.L. Can the formation of pharmaceutical cocrystals be computationally predicted? I. Comparison of lattice energies. *Cryst. Growth Des.* **2009**, *9*, 442–453. [CrossRef]
54. Du, J.J.; Lai, F.; Váradi, L.; Williams, P.A.; Groundwater, P.W.; Platts, J.A.; Hibbs, D.E.; Overgaard, J. Monoclinic paracetamol vs. Paracetamol-4,4′ -bipyridine co-crystal; what is the difference? a charge density study. *Crystals* **2018**, *8*, 46. [CrossRef]
55. Surov, A.O.; Voronin, A.P.; Vasilev, N.A.; Churakov, A.V.; Perlovich, G.L. Cocrystals of Fluconazole with Aromatic Carboxylic Acids: Competition between Anhydrous and Hydrated Solid Forms. *Cryst. Growth Des.* **2020**, *20*, 1218–1228. [CrossRef]
56. Boag, N.M.; Coward, K.M.; Jones, A.C.; Pemble, M.E.; Thompson, J.R. 4,4′-Bipyridyl at 203 K. *Acta Cryst.* **1999**, *C55*, 672–674. [CrossRef]
57. Li, J.-T.; Wang, Y.-L.; Zhou, L.-N.; Wang, J.-K. 3,4-Methylenedioxybenzoic acid. *Acta Cryst.* **2006**, *E62*, 1893–1894. [CrossRef]
58. Wang, Z.; Miller, B.; Mabin, M.; Shahni, R.; Wang, Z.D.; Ugrinov, A.; Chu, Q.R. Cyclobutane-1,3-Diacid (CBDA): A Semi-Rigid Building Block Prepared by [2+2] Photocyclization for Polymeric Materials. *Sci. Rep.* **2017**, *7*, 1–7. [CrossRef]
59. Ghiassi, K.B.; Guenthner, A.J.; Redeker, N.D.; Boatz, J.A.; Harvey, B.G.; Davis, M.C.; Chafin, A.P.; Groshens, T.J. Insights into Melting Behavior of Propyl-Bridged Di(cyanate ester) Monomers through Crystal Packing, Thermal Characterization, and Computational Analysis. *Cryst. Growth Des.* **2018**, *18*, 1030–1040. [CrossRef]
60. Monika; Verma, A.; Tiwari, M.K.; Show, B.; Saha, S. Modulation of Weak Interactions in Structural Isomers: Positional Isomeric Effects on Crystal Packing and Physical Properties and Solid-State Thin-Film Fabrication. *ACS Omega* **2020**, *5*, 448–459. [CrossRef]